Thermochemical Heat Storage Properties of Co_3O_4-X wt % Al_2O_3 and Co_3O_4-X wt % Y_2O_3 Composites (X=1, 2, 5, 8, 10)

Azin Hasanvand, Mehdi Pourabdoli*, Ahmad Ghaderi Hamidi

Department of Materials Engineering, Hamedan University of Technology, P. O. Box: 65155-579, Hamedan, Iran.

ABSTRACT

The effect of Al_2O_3 (1-10 wt %) and Y_2O_3 (1-10 wt %) additions on thermochemical heat storage properties of Co_3O_4/CoO system was investigated by thermogravimetry, XRD, and SEM analyses. Results showed that the addition of Al_2O_3 to Co_3O_4 at constant 8 h mechanical activation improved the redox cycle stability and increased oxygen sorption value and rate. It was found that oxygen sorption and their rate decreased with increasing the alumina content to more than 8 wt %. The formation of the spinel phase and an increase in its amount by increasing the alumina content led to a decrease in the oxygen sorption capacity. SEM studies showed that Al_2O_3 prevented the sintering and particle growth of cobalt oxide particles during reduction and re-oxidation processes. In addition, results showed that the addition of Y_2O_3 in all ranges to Co_3O_4 improved the redox cycle stability of cobalt oxide; however, it significantly decreased the oxygen sorption in the Co_3O_4/CoO system. XRD patterns of a sample containing 10 wt % yttria before the redox process indicated the presence of only Co_3O_4 phase; however, after three redox cycles, other phases including CoO and Y_2O_3 appeared.

1. INTRODUCTION

Nowadays, demand for fossil fuels has risen and rapidly increases every year due to the development of industries and population growth. This rise in demand has led to higher prices of these fuels, greenhouse gas emissions, environmental pollution, and climate change. Therefore, it is necessary to change existing energy production systems and create newer technologies for generating clean energy. Technologies working with solar light and/or heat use solar energy as an abundant renewable source of energy. Moreover, a more efficient way to use solar energy is to store some of this energy to use it during off-sun hours and, then, be able to keep a constant production for industrial processes. Thermal energy storage (TES) is a key feature of concentrating solar power (CSP) plants to match the intermittent energy source supply with the variable electricity demand, improving energy generation dispatch. Therefore, TES technology joint with CSP plants reduces the environmental problems and increases energy efficiency. Among the different types of TES systems (thermochemical, latent heat, and sensible heat storage), the thermochemical heat storage is of particular interest [1-5]. In fact, thermochemical heat storage method could prove own superiority to other methods due to its higher storage capacity, broader operational temperature range, and negligible loss on storage [6].

Transforming thermal energy to chemical energy is not a new idea, but its good coupling possibility with CSP systems recently renewed the interest in it. Among the various CSP technologies, air-operated solar thermal power plants offer the potential of high temperatures and, thus, high thermodynamic conversion efficiencies together with the efficient use of air as heat transfer medium [7].

The use of thermochemical reactions is a promising approach to heat storage applications. Redox-reactions involving multivalent cations have been recently envisaged for high temperature applications. In temperature range of 900-1000 °C, however, where heat storage is required for CSP processes, only few metal oxides with sufficient heat storage capabilities do exist [8].

Materials for thermochemical heat storage to achieve better design and performance should include features such as reactivity, high reaction rates, easy controllability, easy storage, safety, and economic savings [9, 10]. The selected materials are hydrated sulfates, hydrated chlorides, hydroxides, and metal oxides [11-14]. Thermochemical heat storage based on the reduction and re-oxidation of metal oxides has been identified as one of the most feasible approaches for TES at high temperatures [15].

Wong et al. [16] investigated various oxides such as Fe_2O_3, Co_3O_4, Mn_2O_3, Mn_3O_4, and CuO by thermodynamic equations and laboratory analysis of their potential as a thermal energy storage material. Some of these materials were rejected due to the lack of re-oxidation, high prices of materials, and slow kinetics. Co_3O_4 showed relatively suitable kinetics for redox and re-oxidation reactions in comparison with other metal oxides [7, 17].

A report on the redox cycling of Co_3O_4 on several solid supports for implementation in a reactor setup, as well as the combination with Mn_2O_3 in a cascade-energy storage concept, was made. Other approaches, focusing on faster re-oxidation of CoO, concentrate on the spinel-chemistry of Co_3O_4, leading to the formation of binary metal oxides. Material fatigue and mechanical stress were investigated through studies of cycle stability, and related concepts for application in technological processes have already been developed [18]. The redox reactions of Co_3O_4/CoO are as follows [19]:

*Corresponding Author's Email: mpourabdoli@hut.ac.ir (M. Pourabdoli)

$$2Co_3O_4 + \Delta H \leftrightarrow 6CoO + O_2 \quad \Delta H = \pm 205 \frac{kJ}{mol} \qquad (1)$$
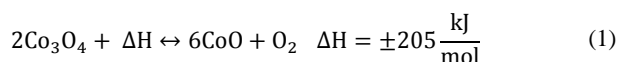
The problem of Co_3O_4 is its sintering during redox reactions results in particle growth and the subsequent decline of thermal energy storage properties. Low melting point of Co_3O_4 (895 °C) facilitates the sintering. Large particles formed after sintering imposes a kinetic barrier against the oxygen transfer during redox reactions. To overcome this problem, the addition of a secondary oxide such as Fe_2O_3, Cu_2O, and Al_2O_3 to cobalt oxide can be useful. The addition of these oxides improves the thermal energy storage properties of cobalt oxide by preventing the sintering of cobalt oxide particles [11].

Nieses et al. [20] studied the effect of Al_2O_3 and Cu_2O additions separately on the cobalt oxide stability. They observed that the addition of alumina was more effective in CoO re-oxidation than copper oxide. Pagkoura et al. [21] used two different mixtures of cobalt oxide and aluminum oxide containing 10 and 4.5 wt % alumina as honeycomb structures and subjected them to thermal cycling. They observed that the addition of aluminum oxide improved the cycle stability of cobalt oxide by preventing the growth of cobalt oxide particles at the expense of a decrease in energy storage density. A mixture of cobalt oxide with other oxides such as MnO, CuO, NiO, MgO was used for thermal energy storage by Carrillo et al. [22]. They observed the best yield by cobalt-manganese system. Agrafiotis et al. [23] used cobalt oxide as a coating of silicon-carbide foam honeycomb cells and investigated the properties of thermal energy storage in this system. They did not observe a significant change in the properties of thermal energy storage in cobalt oxide. However, cobalt oxide coating on silicon-carbide foams can be useful for thermal energy storage in long periods, because these foams produce extremely high oxide stability in thermal cycles.

Despite previous studies, research and reassessment of heat storage materials continues. According to Silakhore et al. [24] studies, the Co_3O_4/CoO, Mn_2O_3/Mn_3O_4, and CuO/Cu_2O pairs have a potential for chemical storage at temperatures of 900 °C to 1000 °C, while no thermochemical reaction was observed for Pb_3O_4 up to a temperature of 550 °C. Zhou et al. [25] focused on the innovative one-dimensional modeling of an energy storage system based on the redox cycle of cobalt oxides (Co_3O_4/CoO), coated on the ceramics honeycomb structures. Experimental data published in the literature by other groups validated the simulation results. This validation proved that this model could simulate the overall thermochemical storage process with reasonable accuracy.

Hasanvand and Pourabdoli [26] studied the kinetics of oxygen desorption from Cobalt oxide containing Al_2O_3 and Y_2O_3. They found that Al_2O_3 containing sample desorbed more oxygen than the Y_2O_3 containing sample in similar conditions. They used a model-free method to calculate the reduction activation energies. They found that activation energy required for reducing Co_3O_4-Al_2O_3 and Co_3O_4-Y_2O_3 samples, depending on conversion fraction (α), is in the range of 40-65 kcal/mol and 25-50 kcal/mol, respectively.

To the best knowledge of the authors, the mechanical activation along with Al_2O_3 and Y_2O_3 addition on cobalt oxide redox behavior has not been reported in the literature. Two aims were pursued from this research work. The first objective was to observe the effect of the addition of alumina and yttria (with different melting point) on preventing the sintering and growth of cobalt oxide particles during redox reactions. The second objective was to study the addition of oxides of metals with the same valence (Al^{+3} and Y^{+3}), but with different ionic radii (0.0535 nm and 0.1019 nm) on the redox behavior of cobalt oxide such as cycle stability, oxygen desorption/absorption value, involved phases, and morphological evolution of Co_3O_4/CoO particles.

2. MATERIALS AND METHOD

Raw materials with the specifications presented in Table 1 were used in this research. Various amounts of alumina and yttria including 1, 2, 5, 8, and 10 wt % were added to Co_3O_4, and the mixture was ball milled for 8 h. The time of 8 h was selected based on our previous studies [27]. Ball milling (mechanical activation) was performed by a planetary ball mill (Restch PM 100) equipped with a steel container (150 mL) and steel balls (diameter of 10 and 20 mm) under air atmosphere. A ball to powder weight ratio of 20, a rotation speed of 300 rpm, and a sample weight of 5 g were used in the ball milling. The 15-minute interval was considered as a rest time between each working hour to avoid the side reactions. For convenience, the samples were encoded, as shown in Table 2.

Thermogravimetry (TG) experiments were conducted on 3.8 g samples. The samples in an alumina crucible were placed inside a quartz tube in a tube furnace (Azar furnace 1250). Then, temperature increased from 600 to 1100 °C for reduction process and the sample weight was recorded in real time using a digital balance (A&D model EK-600i) and software (RS weight A&D) linked and installed on a laptop. The similar procedure was performed for the re-oxidation of the same sample by decreasing the temperature from 1100 to 600 °C. Heating/cooling rate and air flow rate were 10 °C / min and 1340 mL/min, respectively.

Table 1. Specifications of used materials.

Material	Purity (wt %)	Particle size (μm)	Company
Co_3O_4	99.5<	<10	Merck
Al_2O_3	99.5<	<200	Fluka
Y_2O_3	99.5<	<10	Merck

Table 2. Sample codes.

Composition	Code	Composition	Code
Co_3O_4-1 wt % Al_2O_3	CA1	Co_3O_4-1 wt % Y_2O_3	CY1
Co_3O_4-2 wt % Al_2O_3	CA2	Co_3O_4-2 wt % Y_2O_3	CY2
Co_3O_4-5 wt % Al_2O_3	CA5	Co_3O_4-5 wt % Y_2O_3	CY5
Co_3O_4-8 wt % Al_2O_3	CA8	Co_3O_4-8 wt % Y_2O_3	CY8
Co_3O_4-10 wt % Al_2O_3	CA10	Co_3O_4-10 wt % Y_2O_3	CY10

XRD analysis was performed by an X-ray diffractometer (Philips PW1730) with Cu-kα radiation at 25 °C under a step size of 0.05 deg/s, 2θ=10-80°. X'Pert High Score (1.0d) software was used to identify the phases. To investigate the morphology and chemical composition of powders, scanning electron microscopy (SEM) (LMU VEGA//TESCAN) equipped with Energy-dispersive Spectroscopy (EDS) was used. The MIP4 software was used to estimate the average particle size.

3. RESULTS AND DISCUSSION

3.1. As-received cobalt oxide behavior

Figure 1 illustrates the TG curve of as-received cobalt oxide obtained at an air flow rate of 1340 mL/min and a heating/cooling rate of 10 °C/min in three redox cycles. According to this curve, weight loss (oxygen desorption) in the first, second, and third cycles was 4.20, 3.40, and 1.80 wt %, respectively, indicating a decrease in oxygen desorption by increasing the number of redox cycles. Further, Figure 1 shows that an increase in weight (oxygen absorption) in the first, second, and third cycles is 4.20, 2.20, and 0 wt %, respectively. In general, the cycle stability of as-received cobalt oxide declines with increasing the number of redox cycles. This is mainly due to sintering and growth of cobalt oxide particles during the redox process, which increases the distance of oxygen diffusion and makes a kinetic obstacle in the process [16,27].
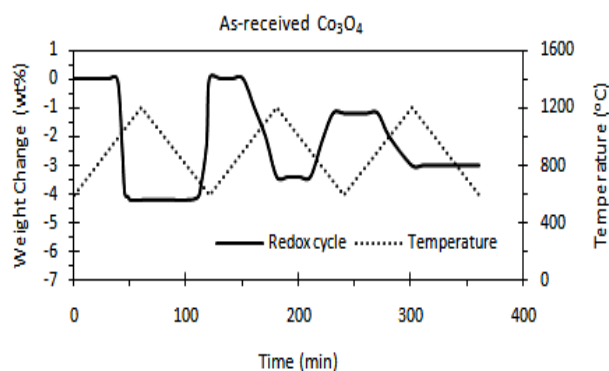

Figure 1. TG curve of as-received cobalt oxide.

3.2. Effect of Al_2O_3 addition on redox behavior of cobalt oxide

A secondary oxide phase addition is a way to improve the redox behavior of cobalt oxide as a heat storage material. The effect of Al_2O_3 addition was investigated by adding 1, 2, 5, 8, and 10 wt % of Al_2O_3 to cobalt oxide and ball milling for 8 h. Results of TG analysis of alumina-containing samples are presented in Figure 2. The results presented in Figure 1 and Figure 2 are compiled in Table 3 that shows the amount and the rate of weight change of samples in the reduction and re-oxidation steps during the first to third cycles. If we exclude the first cycle data due to the instability of the material immediately after mechanical activation, it is seen that:

- Addition of alumina and mechanical activation significantly improve the amount of oxygen sorption relative to as-received cobalt oxide. The reason is that alumina prevents the growth of cobalt oxide particles and their sintering (see part 3.4).
- Weight change decreases with increasing the alumina content. Probably, this is due to increasing the spinel phase ($CoO.Al_2O_3$) formation with increasing the alumina content. The spinel phase is a stable phase that is formed by the reaction of Al_2O_3 and CoO and does not decompose in the temperature range used in the experiments. By forming this phase, some of the cobalt oxide involved will no longer be able to participate in the redox reactions, and it reduces the oxygen desorption/absorption capacity of a sample. A similar phenomenon was observed about the addition of iron oxide to cobalt oxide previously [27]. However, for determining the optimal amount of alumina, both the value and rate of absorption and desorption should be taken into account. More details of spinel phase formation are discussed in Part 3.3.

- Desorption/absorption value improves with increasing the redox cycles. Probably, some of the spinel is likely to decompose with the continuation of the redox process in successive cycles and released cobalt oxide participates in the redox reactions.

By comparing the reduction and re-oxidation data in Table 3, it is seen that weight change in the re-oxidation step is the same as the weight change in the reduction step in each individual cycle. It is implied that redox cycle stability in each cycle is established. Moreover, weight loss rate in the reduction step of all cycles is more than weight increase rate in the re-oxidation step. This is likely to be due to an increase in the size of cobalt oxide particles during the reduction step, thereby increasing the diffusion distance of oxygen atoms and thus increasing the time of re-oxidation process [11, 27-29].
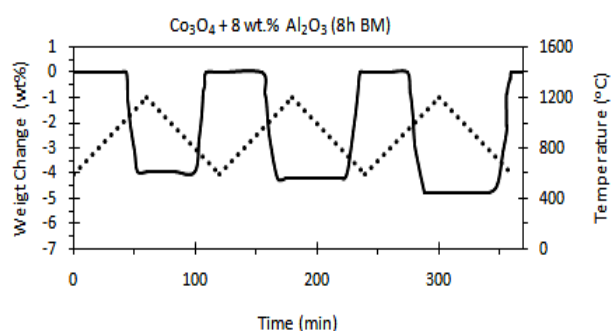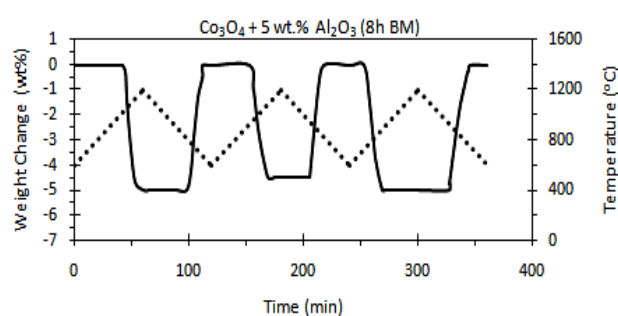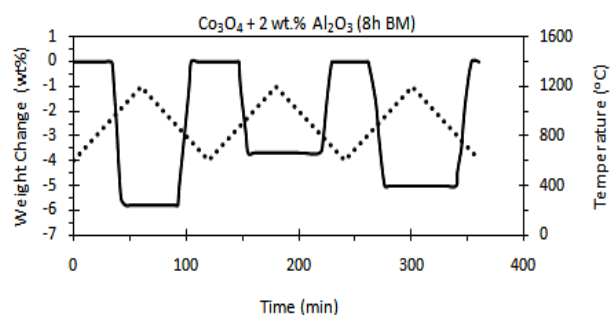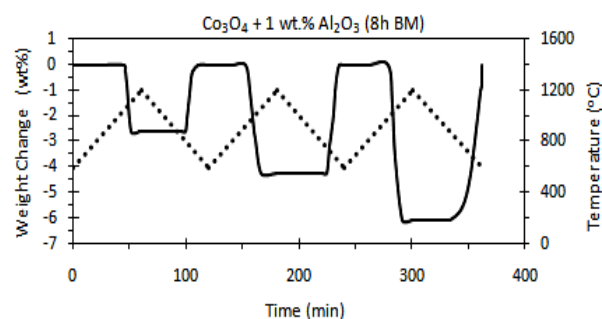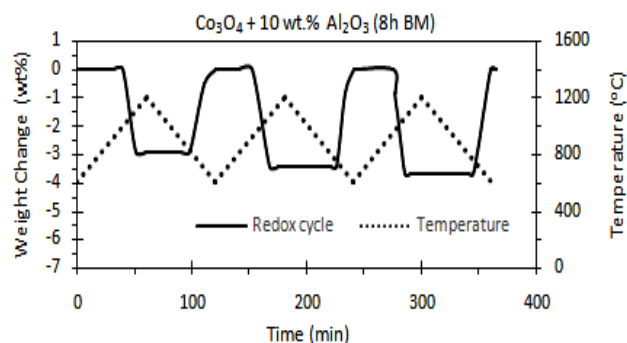
Figure 2. TG curves of CA1, CA2, CA5, CA8, and CA10 samples.

The reduction rate of re-oxidation in the first and second cycles shows a nearly identical trend with increasing of alumina content, although by increasing amounts of alumina, the rate of reduction/re-oxidation in some samples does not directly correlate with the increase of alumina content that is related to the instability of material after the mechanical activation. It seems that, in the third cycle, due to the stability of the material, uniformity has increased in the rates of reduction and re-oxidation. By comparing the rate of reduction and re-oxidation, it can be seen that in the alumina range of 1 to 8 wt %, the rates are more favorable and samples containing lower alumina content have relatively shown a better performance in higher redox cycles (third cycle). This could be due to the decrease of CoO and Al_2O_3 reaction as the spinel phase.

TG curves of alumina-containing samples (Figure 2) in comparison with TG curve of as-received cobalt oxide (Figure 1) show that the addition of alumina improves the redox cycle stability. Pagkoura et al. [21] showed that although the addition of alumina decreased the ability of heat energy storage in cobalt oxide, it improved the cycle stability (10 cycles) of cobalt oxide by preventing the particles growth.

3.3. Phase analysis of alumina-containing samples

XRD patterns of CA1, CA5, CA10 and as-received cobalt oxide samples are shown in Figure 3. From the XRD patterns in Figure 3, it is clear that, by ball milling, the width of the peaks has increased, which results from the crystallite size reduction [30, 31]. Unfortunately, the peaks of spinel phase ($CoAl_2O_4$) and Co_3O_4 are very close and overlapping. That is why it is very difficult to distinguish the peaks of these two phases. However, a careful examination by the software showed that spinel phase peaks were in XRD patterns of CA5 and CA10 samples. It is noteworthy that the largest spinel peak in the CA5 sample clearly appears after the redox process because of sample annealing during redox. In addition, the largest spinel peak in CA10 is clearly seen before the redox because the amount of spinel phase in this sample is high due to high alumina content and can easily be detected by the XRD. Moreover, in diffraction patterns, the peaks of the CoO phase do not appear, which means the absence of this phase in the composition of the samples. Much of this phase probably combines with alumina and creates the spinel phase ($CoO.Al_2O_3$).

The presence of spinel phase, due to its higher decomposition temperature (above 1690 °C), leads to a decline in oxygen sorption value [21]. The presence of spinel peaks in the XRD pattern of CA5 sample after the redox process indicates that at least apart of spinel phase has not

been decomposed during the redox process. According to Table 3, the oxygen sorption values in the sample containing 10 wt % Al_2O_3 is lower than the rest of samples due to containing higher spinel phase. Further, in the XRD pattern of CA10 sample, peak intensity of $CoAl_2O_4$ is more intense than the rest of samples. Therefore, the formation of $CoAl_2O_4$ phase is responsible for the decline in redox behavior. Perhaps, the question remains if as-received cobalt oxide is Co_3O_4 and that there is no CoO in combination with Al_2O_3 that forms spinel. In response to this question, Nekokar et al. [27] reported that some CoO is formed during ball milling.
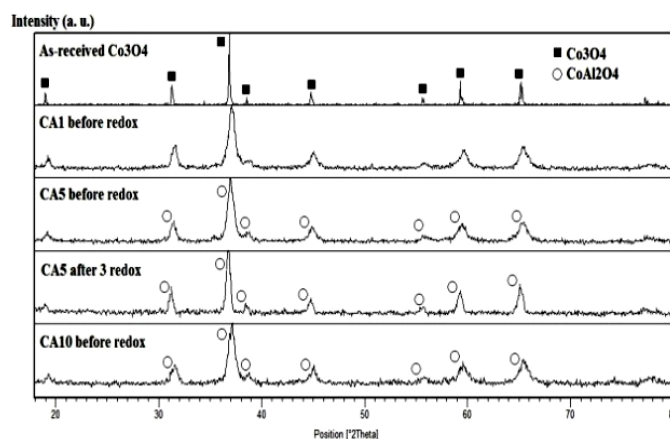

Figure 3. XRD patterns of as-received cobalt oxide, CA1, CA5, and CA10 samples.

Table 3. Weight change value and rate during the first to third cycles for alumina-containing samples.

Alumina content (wt %)	Weight change (wt %)						Weight change rate (wt % / min)					
	Cycle 1		Cycle 2		Cycle 3		Cycle 1		Cycle 2		Cycle 3	
	Red	Oxid	Red	Oxid	Red	Oxid	Red	Oxid	Red	Oxid	Red	Oxid
0	4.20	4.20	3.40	2.20	1.80	0.00	0.37	0.18	0.11	0.11	0.05	0.00
1 (CA1)	2.70	2.70	4.20	4.20	6.00	6.00	0.44	0.26	0.30	0.29	0.46	0.21
2 (CA2)	5.78	5.78	3.67	3.67	5.00	5.00	0.52	0.40	0.43	0.36	0.34	0.26
5 (CA5)	5.00	5.00	4.50	4.50	5.00	5.00	0.31	0.29	0.28	0.27	0.34	0.27
8 (CA8)	3.94	3.94	4.21	4.21	4.74	4.74	0.39	0.13	0.33	0.26	0.33	0.25
10 (CA10)	2.89	2.89	3.42	3.42	3.68	3.68	0.14	0.12	0.15	0.13	0.33	0.24

As mentioned earlier, mechanical activation reduces the size of crystallites, and this phenomenon appears as a peak broadening in the XRD patterns. Reducing the crystallite size is equivalent to increasing the grain boundaries, considered as a suitable place for oxygen diffusion due to the lack of crystalline order. Although this only contributes to the kinetics in the initial cycle, crystallites grow and their positive effect is eliminated in longer cycles due to high temperatures.

3.4. Study of particle morphologies

SEM images of as-received Co_3O_4, 8-hour mechanical activated Co_3O_4, and CA5 samples before and after redox are shown in Figure 4. It is clear that although CA5 sample is subjected to the three redox cycles, its particle growth after redox is less than the as-received cobalt oxide subjected to one cycle redox. Therefore, Al_2O_3 addition plays an important role in reducing the particle sintering and, consequently, improves the cycle stability of the redox reactions. Table 4 shows the

average particle size of as-received Co_3O_4, an 8-hour mechanical activated Co_3O_4, and CA5 samples before and after redox. According to Figure 4 and Table 4, the average particle size of the 8-hour mechanical activated cobalt oxide has increased to 3.50μm after one cycle redox, while the average particle size of CA5 sample increased to 2.50 μm after three redox cycles. Further, the average particle size of as-received cobalt oxide before redox was 1.50 μm; however, after one cycle redox, it increased to 2.50 μm. Therefore, it is clear that the addition of alumina to cobalt oxide slows down the growth of the particles during the redox process. As is seen in Figure 4, without the alumina addition, the particles of the 8-hour mechanical activated Co_3O_4 have grown much higher than as-received Co_3O_4. However, with the addition of alumina, the CA5 sample somewhat maintains own particle size during the redox process. In other words, the addition of alumina retains the positive effect of the mechanical activation process (fine particle size).

As discussed earlier, the main problem with the use of cobalt oxide for thermal energy storage is the weak cycle stability due to particle growth and sintering in the redox process. Therefore, particle morphology also confirms the positive role of alumina addition in preventing the sintering and particles growth of cobalt oxide particles.
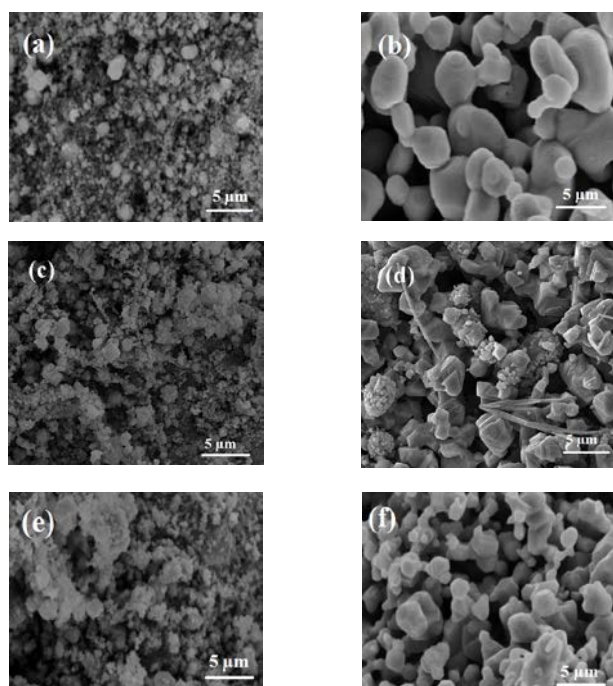

Figure 4. SEM images of as-received Co_3O_4, mechanical activated Co_3O_4 (8 h BM), and CA5 samples before and after redox; (a) Co_3O_4–8 h BM before redox, (b) Co_3O_4–8 h BM after one redox cycle, (c) CA5 before redox, (d) CA5 after three redox cycles, (e) as-received Co_3O_4 before redox, and (f) as-received Co_3O_4 after redox.

**Table 4.** Average particle size of as-received Co_3O_4, mechanical activated Co_3O_4 (8 h BM), and CA5 samples.

Alumina wt %	BM time (h)	Particle size before redox (μm)	Particle size after redox (μm)
0	0	1.50	2.50 (after 1 cycle)
0	8	0.75	3.50 (after 1 cycle)
5	8	0.96	2.50 (after 3 cycles)

3.5. Effect of Y_2O_3 addition on cobalt oxide behavior

To investigate the effect of yttria on cobalt oxide redox behavior, 1, 2, 5, 8, and 10 wt % of Y_2O_3 were added to cobalt oxide, and the resulting mixture was ball billed for 8 h. The samples were then subjected to three redox cycles at a heating/cooling rate of 10 °C / min and an airflow rate of 1340 ml/min. TG results of the samples are shown in Figure 5.

The aim of yttria addition to cobalt oxide was to evaluate the effect of secondary oxide melting point and ionic radius on redox behavior of cobalt oxide. These parameters are important because the additive phase with a high melting point placed around the cobalt oxide particles can prevent the adhesion and sintering of the cobalt oxide particles. Further, it has been claimed that a higher ionic radius of metal cation involved in secondary metal oxide led to a lattice strain, and an electrical charge imbalance in cobalt oxide structure resulted in an increase in atomic vacancy facilitating the transfer of oxygen atoms [11].

Table 5 shows the weight change and rate values extracted from Figure 5. According to Table 5, if only the second and third cycles are taken into account, the amount of oxygen sorption of samples containing 1-10 wt % yttria isin the range of 0-2.89 wt %. Therefore, the addition of yttria to cobalt oxide has a negative effect on oxygen sorption. It must be mentioned that the addition of yttria improves redox cycle stability. However, because of an intense decline in oxygen sorption, the improvements in cycle stability of cobalt oxide could not be compensated. This decline is attributed to the formation of stable compounds of yttrium oxide and cobalt oxide, which cannot decompose at the experiment temperatures.
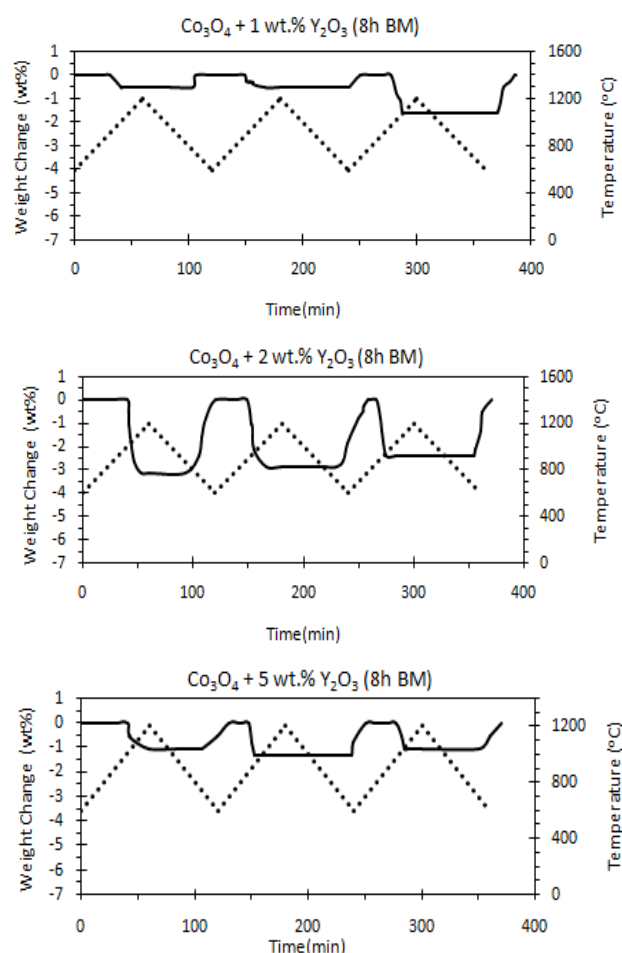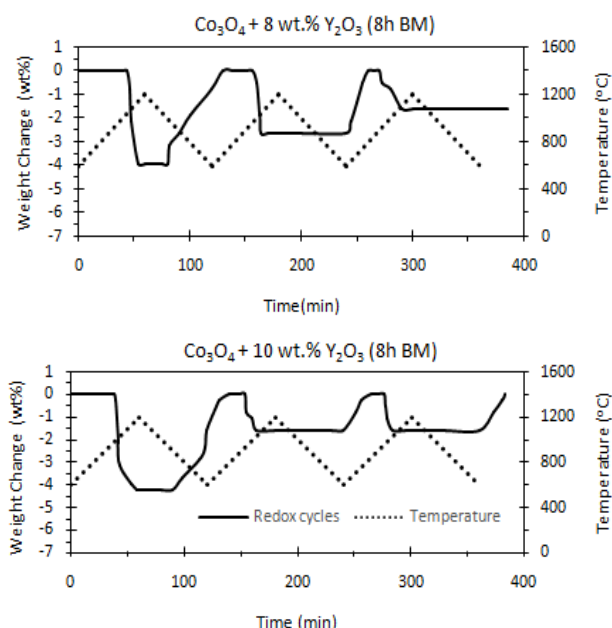
Figure 5. TG curves of CY1, CY2, CY5, CY8, and CY10 samples.

Table 5. Weight change value and rate during the first to third cycles for yttria-containing samples.

Yttria content (wt %)	Weight change (wt %)						Weight change rate (wt % / min)					
	Cycle 1		Cycle 2		Cycle 3		Cycle 1		Cycle 2		Cycle 3	
	Red	Oxid	Red	Oxid	Red	Oxid	Red	Oxid	Red	Oxid	Red	Oxid
0	4.20	4.20	3.40	2.20	1.80	0.00	0.37	0.18	0.11	0.11	0.05	0.00
1 (CA1)	0.52	0.52	0.53	0.53	1.58	1.58	0.04	0.01	0.02	0.04	0.15	0.09
2 (CA2)	3.15	3.15	2.89	2.89	2.73	2.73	0.24	0.10	0.15	0.11	0.26	0.15
5 (CA5)	1.15	1.15	1.32	1.32	1.15	1.15	0.04	0.04	0.20	0.09	0.14	0.05
8 (CA8)	3.14	3.14	2.64	2.64	1.58	0.00	0.30	0.07	0.31	0.11	0.07	0.00
10 (CA10)	4.21	4.21	1.57	1.57	1.58	1.58	0.19	0.09	0.12	0.06	0.19	0.06

It was expected of Y_2O_3 to be more effective in facilitating the diffusion of oxygen atoms due to the higher difference at anionic radius of Y^{3+} and Co^{+2} /Co^{+3} than that of Al^{+3} and Co^{+2}/Co^{+3} (Table 6), resulting in large potential for the distortion of cobalt oxide structure. Moreover, Y_2O_3 melting point is higher than Al_2O_3 and could be more effective in preventing the sintering and growth of cobalt oxide particles. However, results did not validate these hypotheses in practice, and showed that other parameters such as secondary oxide reactability with cobalt oxide, decomposition temperature of new formed compounds, and various ions diffusion capability in involved oxide structures affected the secondary oxide performance. The particle morphology in SEM images (Figure 6) illustrates this very well. The average particle size according to SEM images for CY5 is 0.89 µm before redox; however, after three redox cycles, the particle size of this sample reaches about 6 µm that is more than that of as-received Co_3O_4 and 8-h mechanical activated Co_3O_4 (Table 4). Therefore, the Y_2O_3 addition has increased the size of cobalt oxide particles severely. The SEM images (Figure 4 and Figure 6) show that the addition of yttrium oxide not only did not have any effect on preventing particle growth and sintering of cobalt oxide, but also increased it. According to EDS analysis of two particles in Table 7, the particles shown

with D in Figure 6 are rich in yttrium. These particles are formed by the diffusion of cobalt atoms in the structure of yttrium oxide.

Table 6. Ion radius and melting point of cobalt oxides, aluminum oxide, and yttrium oxide [32, 33].

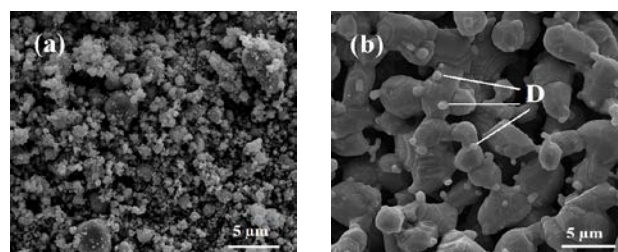| Compound	Lattice parameter (nm)	Ion	Ionic radius (nm)	Melting point ($^\circ$C)
Co_3O_4	0.8084	Co^{+3}	0.06	895
CoO	0.4260	Co^{+2}	0.07	1933
Al_2O_3	---	Al^{+3}	0.053	2072
Y_2O_3	1.062	Y^{+3}	0.09	2425
---	---	O^{-2}	0.14	---

Figure 6. SEM images of CY5; (a) before redox and (b) after three redox cycles.

Table 7. EDS analysis of spherical particles shown in SEM images in Figure 6.

Element (wt %)	Point	
	Particle 1	Particle 2
Oxygen	14.70	25.84
Cobalt	62.22	58.29
Yttrium	23.07	15.86

It was expected of Y_2O_3 to be more effective in facilitating the diffusion of oxygen atoms due to the higher difference at anionic radius of Y^{3+} and Co^{+2} /Co^{+3} than that of Al^{+3} and Co^{+2}/Co^{+3} (Table 6), resulting in large potential for the distortion of cobalt oxide structure. Moreover, Y_2O_3 melting point is higher than Al_2O_3 and could be more effective in preventing the sintering and growth of cobalt oxide particles. However, results did not validate these hypotheses in practice, and showed that other parameters such as secondary oxide react ability with cobalt oxide, decomposition temperature of new formed compounds, and various ions diffusion capability in involved oxide structures affected the secondary oxide performance. The particle morphology in SEM images (Figure 6) illustrates this very well. The average particle size according to SEM images for CY5 is 0.89 µm before redox; however, after three redox cycles, the particle size of this sample reaches about 6 µm that is more than that of as-received Co_3O_4 and 8-h mechanical activated Co_3O_4 (Table 4). Therefore, the Y_2O_3 addition has increased the size of cobalt oxide particles severely. The SEM images (Figure 4 and Figure 6) show that the addition of yttrium oxide not only did not have any effect on preventing particle growth and sintering of cobalt oxide, but also increased it. According to

EDS analysis of two particles in Table 7, the particles shown with D in Figure 6 are rich in yttrium. These particles are formed by the diffusion of cobalt atoms in the structure of yttrium oxide.

Figure 7 shows the phase analysis of CY1, CY5, CY10, and as-received cobalt oxide samples. The comparison of XRD patterns of CY10 sample before and after redox suggests that although only $Co_3O_4$was detected by XRD before redox, after three redox cycles, other phases in the sample including CoO, Co_3O_4, and Y_2O_3 appeared. The presence of Co_3O_4 phase in the sample after redox is logical, but the CoO phase in CY10 sample after redox is not logical. It is interesting that Y_2O_3 and CoO peaks did not appear before the redox process of CY10 sample; however, those peaks appeared in XRD pattern after the redox process. It seems that a portion of yttrium cations during the ball milling process has been solved in the structure of the Co_3O_4 (the structure before redox); therefore, the yttrium oxide peaks are not recognizable before the redox process. By converting Co_3O_4 to CoO during the redox process, yttrium cations exit the Co_3O_4 structure and forms again a separate phase as Y_2O_3. Further, due to the high temperature of the redox process, various (yttrium and cobalt) cations can diffuse into the structure of the existing compounds (CoO and Y_2O_3). Since yttrium cation (Y^{+3}) has a large ionic radius, it cannot diffuse into the CoO structure; however, cobalt cation (Co^{+2}) due to small ionic radius can diffuse into yttrium oxide structure (spherical particles, D, in Figure 6). Exhaust of cobalt cations from the CoO structure results in an increase in the concentration of oxygen anions in the CoO structure, which means that the structure cannot absorb oxygen (anionic atoms) due to the concentration of high oxygen anions in the structure. That is why in the XRD pattern of CY10 sample after the redox process, the CoO is the main phase. Therefore, only some free Co_3O_4 can be incorporated in the redox process. For this reason, the oxygen sorption value in these samples is low according to Figure 5.
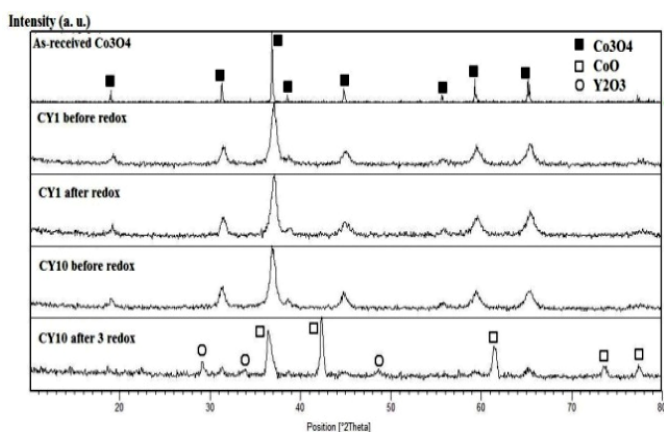

Figure 7. XRD patterns of as-received cobalt oxide, CY1, CY5, and CY10 samples.

3.6. Comparison of Y_2O_3 and Al_2O_3 additives performance

Although, it was expected that Y_2O_3 performance be better than alumina due to the higher melting point and ionic radius. However, the results showed that the addition of alumina significantly increased the amount and rate of oxygen sorption during the reduction and re-oxidation steps; in addition, it increased the redox cycle stability of cobalt oxide. It is

implied that the addition of alumina improves the redox behavior of cobalt oxide. However, the addition of yttria improved the redox cycle stability of cobalt oxide, but it destroyed the oxygen sorption. This disadvantage is the reason why yttria is considered as an improper additive.

4. CONCLUSIONS

The main problem with the use of cobalt oxide for thermal energy storage is weak cycle stability due to particle growth and sintering during the redox process. Alumina addition to cobalt oxide improved the cobalt oxide redox behavior, because it prevented the growth of cobalt oxide particles during redox reactions. However, the addition of alumina excess than 5 wt % reduced the oxygen sorption capacity due to the formation of large amount $CoAl_2O_4$ spinel phase. The addition of Y_2O_3 in all ranges to Co_3O_4improvedthe redox cycle stability of cobalt oxide; however, it significantly decreased the oxygen sorption in the Co_3O_4/CoO system. XRD patterns of a sample containing 10 wt % yttria before the redox process indicated the presence of only Co_3O_4 phase; however, after three redox cycles, other phases including CoO and Y_2O_3 appeared. SEM images showed the growth of intense particles after redox in the Y_2O_3 containing samples. As a result, unlike Y_2O_3, Al_2O_3 improved the cobalt oxide thermochemical heat storage properties. Results showed that other parameters such as secondary oxide reacting ability with cobalt oxide, decomposition temperature of newly formed compounds, and various ions diffusion capability involved in oxide structures affected the secondary oxide performance.

REFERENCES

1. Rasthal, J.E. and Drennen, T.E., Pathways to a hydrogen future, 3rd ed., Elsevier, UK, (2007), 243-350.

2. Rahm, D., Sustainable energy and the states, essay on politics markets and leadership, 1st ed., McFarland, North Carolina, (2002), 102-323.

3. Fuglestvedt, J.S., Hailemariam, K. and Stuber, N.,"Alternatives to the global warming potential for comparing climate impacts of emissions of greenhouse gases", *Climate Change*, Vol. 68, (2005), 281-302. (https://doi.org/10.1007/s10584-005-1146-9).

4. Abedini, A.H. and Rosen, M.A.,"A critical review of thermochemical energy storage systems", *The Open Renewable Energy*, Vol. 4, (2011), 42-46. (DOI: 10.2174/1876387101004010042).

5. André, L., Abanades, S. and Flamant, G., "Screening of thermochemical systems based on solid-gas reversible reactions for high temperature solar thermal energy storage", *Renewable and Sustainable Energy Reviews*, Vol. 64, (2016), 703-715. (https://doi.org/10.1016/j.rser.2016.06.043).

6. Wokon, M., Block, T., Nicolai, S., Linder M. and Schmücker M., "Thermodynamic and kinetic investigation of a technical grade manganese-iron binary oxide for thermochemical energy storage", *Solar Energy*, Vol. 153, (2017), 471-485. (https://doi.org/10.1016/j.solener.2017.05.045).

7. Tescari, S., Singh, A., Agrafiotis, C., de Oliveira, L., Breuer, S., Schlögl-Knothe, B., Roeb, M. and Sattler, C., "Experimental evaluation of a pilot-scale thermochemical storage system for a concentrated solar power plant", *Applied Energy*, Vol. 189, (2017), 66-75. (https://doi.org/10.1016/j.apenergy.2016.12.032).

8. Block, T., Knoblauch, N. and Schmucker, M., "The cobal-oxide/iron-oxide binary system foruse as high temperature thermochemical energy

storage material", **Thermochimica Acta**, Vol. 577, (2014), 25-32. (https://doi.org/10.1016/j.tca.2013.11.025).

9. Karagiannakis, G., Pagkoura, C., Halevas, E., Baltzopoulou, P. and Konstandopoulos, A.G., "Cobalt/cobaltous oxide based honeycombs for thermochemical heat storage in future concentrated solar power installations", **Solar Energy**, Vol. 133, (2016), 394-407. (https://doi.org/10.1016/j.solener.2016.04.032).

10. Lefebvre, D. and Tezel, F., "A review of energy storage technologies with a focus on adsorption thermal energy storage processes for heating applications", **Renewable and Sustainable Energy Reviews**, Vol. 67, (2017), 116-125. (https://doi.org/10.1016/j.rser.2016.08.019).

11. U.S. Department of Energy, Thermochemical heat storage for concentrated solar power, General atomic project 2011, GA-C27137.

12. Miyaoka, H., Ichikawa, T. and Kojima, Y., "Thermochemical energy storage by water splitting via redox reaction of alkali metals", **Energy Procedia**, Vol. 49, (2014), 927-934. (https://doi.org/10.1016/j.egypro.2014.03.100).

13. Jong, A., Trausel, F., Finck, C., Vliet, L. and Cuypers, R., "Thermochemical heat storage-system design issues", **Energy Procedia**, Vol. 48, (2014), 309-319. (https://doi.org/10.1016/j.egypro.2014.02.036).

14. Tescari, S., Agrafiotis, C., Breuer, S., de Oliveira, L., Neises-von Puttkamer, M., Roeb, M. and Sattler, C., "Thermochemical solar energy storage via redox oxides", **Energy Procedia**, Vol. 49, (2014), 1034-1043. (https://doi.org/10.1016/j.egypro.2014.03.111).

15. Haseli, P., Jafarian, M. and Nathan, G.J., "High temperature solar thermochemical process for production of stored energy and oxygen based on CuO/Cu$_2$O redox reactions", **Solar Energy**, Vol. 153, (2017), 1-10. (https://doi.org/10.1016/j.solener.2017.05.025).

16. Wong, B., Brown, L., Schaube, F., Tamme, R. and Sattler, C., "Oxide based thermo-chemical heat storage", **Proceedings of the 16th Solar PACES International Symposium**, Perpignan, France, (2010).

17. Muroyama, A.P., Schrader, A.J. and Loutzenhiser, P.G., "Solar electricity via an air Brayton cycle with an integrated two-step thermochemical cycle for heat storage based on Co$_3$O$_4$/CoO redox reactions II: Kinetic analysis", **Solar Energy**, Vol. 122, (2015), 409-418. (https://doi.org/10.1016/j.solener.2015.08.038).

18. Müller, D., Knoll, C., Artner, W., Harasek, M., Gierl-Mayer, C., Welch, J.M., Werner, A. and Weinberger, P., "Combining in-situ X-ray diffraction with thermogravimetry and differential scanning calorimetry - An investigation of Co$_3$O$_4$, MnO$_2$ and PbO$_2$ for thermochemical energy storage", **Solar Energy**, Vol. 153, (2017), 11-24. (https://doi.org/10.1016/j.solener.2017.05.037).

19. Pardo, P., Deydier, A., Anxionnaz-Minvielle, Z., Rouge, S., Cabassud, M. and Cognet, P., "A review on high temperature thermochemical heat energy storage", **Renewable and Sustainable Energy**, Vol. 32, (2014), 591-610. (https://doi.org/10.1016/j.rser.2013.12.014).

20. Neises, M., Tescari, S., de Oliveira, L., Roeb, M., Sattler, C. and Wong, B., "Solar-heated rotary kiln for thermochemical energy storage", **Solar Energy**, Vol. 86, (2014), 3040–3048. (https://doi.org/10.1016/j.solener.2012.07.012).

21. Pagkoura, C., Karagiannakis, G., Zygogianni, A. and Woodhead, J.W., "Cobalt oxide based structured bodies as redox thermochemical heat storage medium for future CSP plants", **Solar Energy**, Vol. 108, (2014), 146-163. (https://doi.org/10.1016/j.solener.2014.06.034).

22. Carrillo, A., Serrano, D., Pizarro, P. and Coronado, J.M., "Thermochemical heat storage at high temperature using Mn$_2$O$_3$/Mn$_3$O$_4$ system", **Energy Procedia**, Vol. 73, (2015), 263-271. (https://doi.org/10.1016/j.egypro.2015.07.686).

23. Agrafiotis, C., Roeb, M., Schmucker, M. and Sattler, C., "Exploitation of thermochemical cycles based on solid oxide redox system for thermochemical storage of solar heat", **Solar Energy**, Vol. 102, (2014), 189-211. (https://doi.org/10.1016/j.solener.2013.12.032).

24. Silakhori, M., Jafarian, M., Arjomand, M. and Nathar, G.J., "Thermogravimetric analysis of Cu, Mn, Co, and Pb oxides for thermochemical energy storage", **Journal of Energy Storage**, Vol. 23, (2019), 138-147. (https://doi.org/10.1016/j.est.2019.03.008).

25. Zhou, X., Mahmood, M., Chen, J., Yang, T., Xiao, G. and Ferrari, M., "Validated model of thermochemical energy storage based on cobalt oxides", **Applied Thermal Engineering**, Vol. 159, (2019), In press. (https://doi.org/10.1016/j.applthermaleng.2019.113965).

26. Hasanvand, A. and Pourabdoli, M., "Theoretical thermodynamics and practical kinetics studies of oxygen desorption from Co$_3$O$_4$-5 wt % Al$_2$O$_3$ and Co$_3$O$_4$-5 wt % Y$_2$O$_3$ composites", **Journal of Particle Science & Technology**, Vol. 5, (2019), 13-21. (DOI: 10.22104/JPST.2019.3236.1138).

27. Nekokar, N., Pourabdoli, M., Ghaderi Hamidi, A. and Uner, D., "Effect of mechanical activation on thermal energy storage properties of Co$_3$O$_4$/CoO system", **Advanced Powder Technology**, Vol. 2, (2018), 333-340. (https://doi.org/10.1016/j.apt.2017.11.020).

28. Block, T. and Schumucker, M., "Metal oxides for thermochemical energy storage", **Solar Energy**, Vol. 126, (2016), 195-207. (https://doi.org/10.1016/j.solener.2015.12.032).

29. Levenspiel, O.,Chemical reaction engineering, 3rd ed., John Wiley & Sons, USA, (1999), 345-368.

30. Suryanarayana, C., Mechanical alloying and milling, CRC Press, (2004), 127-300.

31. Cullity, B.D. and Stock, S.R., Elements of X-ray diffraction, 3rd ed., Pearson, UK, (2013), 245-342.

32. Neikov, O.D. and Naboychenko, S., Handbook of non-ferrous metal powders, 1st ed., Elsevier, (2008), 323-389.

33. Mao, Y., Engels, J., Houben, A., Rasinski, M., Steffens, J., Terra, A., Linsmeier, Ch. and Coenen, J.W., "The influence of annealing on yttrium oxide thin film deposited by reactive magnetron sputtering: Process and microstructure", **Nuclear Materials and Energy**, Vol. 10, (2017), 1-8. (https://doi.org/10.1016/j.nme.2016.12.031).